روابط فازی و تاریخچه واکنش‌های دگرگونی در سنگهای رسی دگرگون شده کلریتوئیددار و بدون کلریتوئید، منطقه ماهنشان، شمالغرب ایران

عادل ساکی¹، محسن موذن²، منصور مجتهدی²، رولند اوبرهانسلی³

۱-گروه زمین شناسی دانشگاه شهید چمران اهواز
۲-گروه زمین شناسی دانشکده علوم دانشگاه تبریز
۳ - انستیتو علوم زمین دانشگاه پتسدام، آلمان
پست الکترونیکی: *adel_saki@yahoo.com*

چکیده: مجموعه کانیها، بافتهای واکنشی و ترکیب کانیهای سنگهای رسی دگرگون شده منطقه جنوب‌غرب ماهنشان واقع در شمالغرب ایران به منظور بازسازی تاریخچه واکنشهای دگرگونی، مورد بررسی قرار گرفته است. تاریخچه واکنشها در سنگهای رسی دگرگون شده بدون کلریتوئید و کلریتوئیددار کمپلکس ماهنشان جهت مطالعه روابط فازی با استفاده از نمودارهای فازی AFM, AFMn بر اساس ترکیب واقعی و ایزوگراد کانیها بررسی شده است. کانیهای اصلی در سنگهای رسی دگرگونی شده گرانیتی بدون کلریتوئید در بلند پرچین عبارتند از، گارنت، استارولیت، آندالوزیت، کیانیت، فیبرولیت، بیوتیت، مسکویت و کوارتز. در این سنگها ایزوگرادها جزء سری دگرگونی باروین هستند. سنگهای رسی دگرگون شده کلریتوئیددار منطقه دارای کانیهای گارنت، استارولیت، کلریت، مسکویت، کلریتوئید و کوارتز هستند. در این سنگها ایزوگرادها شبیه سری دگرگونی باروین نبوده ولی اولین ظهور کانی کلریتوئید در ترکیب سنگهای با آلومینیم بالا را نشان می‌دهد. روابط فازی در نمودارهای AFM و AFMn برای شناخت واکنشهای دگرگونی تشکیل دهنده کانیها در هر دو دسته سنگهای کلریتوئیددار و بدون کلریتوئید مورد استفاده قرار گرفته‌اند.

واژه‌های کلیدی: کمپلکس ماهنشان، سنگهای رسی دگرگون شده، کلریتوئید، روابط فازی، تایخچه واکنشها، سری باروین.

Phase relations and reaction histories of chloritoid-free and chloritoid-bearing metapelites from the Mahneshan area, NW Iran

A. Saki [1], M. Moazzen[2], M. Modjtahedi[2], R. Oberhänsli[3]

1- Depatrmant of Geology, Shahid Chamran University, Ahvaz, Iran
1- Depatrmant of Geology, University of Tabriz, 51664 Tabriz, Iran
3- Institut für Geowissenschaften, Universität Potsdam, Germany
E-mail: adel_saki@yahoo.com

Abstract: Mineral assemblages, reaction textures and mineral composition of the metapelitic rocks from the Mahneshan area in NW Iran are studied to reconstruct the reaction history of the rocks. The phase relation on the real mineral chemistry AFM, AFMn compatibility diagrams and mineral isograds in chloritoid-free and chloritoid-bearing metapelites of Mahneshan Complex were studied in order to determine the reaction history. The main minerals in the graphitic metapelites (chloritoid-free schist) of the Bolandparchin are garnet, staurolite, andalusite, kyanite, fibrolite, biotite, muscovite and quartz. The isograds are typical Barrovian. Chloritoid-bearing metapelites of the area contain the minerals garnet, staurolite, chlorite, muscovite, chloritoid and quartz. The isograds are not compatible with Barrovian type, but reflect the first appearance of chloritoid in the aluminous bulk compositions. Phase relations on the AFM and AFMn compatibility diagram are used to find the metamorphic reactions in both chloritoid-bearing and chloritoid-free rocks.

Keywords: *Mahneshan Complex, metapelites, chloritoid, phase relation, reactions history, Barrovian type.*

1- Introduction

The chemical system K_2O-FeO-MgO-Al_2O_3-SiO_2-H_2O (KFMASH) was used to study the compatibility of the coexisting phases in the Mahneshan metapelites [1]). In this paper, we assume an equilibrium or at least a close to equilibrium condition for crystallization of different metamorphic minerals in the metapelitic rocks of the Mahneshan area.

The observed mineral assemblages, the analysis of reaction textures and the mineral compositions are used to reconstruct the reaction history of the rocks in the Mahneshan Complex. Based on field and petrography studies, four metamorphic phases have affected the area. The first phase (M_1) has been a regional metamorphic event, crystallizing garnet, biotite and muscovite. Inclusion trails within andalusite, staurolite and garnet are developed, which help to determine the relative chronology of the metamorphic and deformational phases. The second phase (M_2) has formed new minerals such as kyanite, fibrolite, staurolite, andalusite and garnet. The third phase (M_3) is contact metamorphism around younger igneous intrusions, which has produced post deformational andalusite and garnet. The last metamorphic phase (M_4) is retrograde and post-magmatic, which has affected M_1, M_2 and M_3 metamorphic assemblages, overprinting schistosities (both S_1 and S_2) of the rocks.

2- Geological setting

The area chosen for this study is located in NW of Mahneshan town in Zanjan province of Iran. The area is limited to geographical Latitudes of 36° 30′ to 37° 00′N and Longitudes of 47 ° 07′ to 47 ° 45′E (Fig.1). The Mahneshan Complex is located within the Alpine-Himalayan orogenic system of western Asia [2], [3]. Probably, the main geological

features of the area are formed during Pan African orogeny similar to central Iranian block (e.g. [4]).

In the northern part of the Takab quadrangle (Mahneshan Complex is the central part of the Takab quadrangle), a sedimentary sequence (more than 1300 m in thickness) is exposed and ranging in ages from Precambrian, Cretaceous, Eocene, Oligocene-Miocene to post-Miocene [5]. Emplacement of Precambrian and Palaeozoic rocks under the sedimentary and volcanic rocks with Oligo-Miocene age is brought up an old horst (Gor Gor - Belgheys and Ghebleh Dagh horst). This horst with a trend of NW-SE extends from N to S of the area (Fig.2).The western border of this horst is a reverse fault (Gainarjah- Chartag fault) with depression of Shirmard and Eastern border is Pari basin. The base complex is formed of Precambrian rocks which are exposed in the central part of the Mahneshan area.

3- Petrography and deformation
3.1. Structural relations and petrofabric features of pelitic rocks of the study area

Microstructure and petrographic features and field relations show that the formation of Mahneshan metamorphic complex is poly-metamorphic with four metamorphic phases (M_1, M_2, M_3 and M_4) and at least two deformational phases (D_1 and D_2). A poly-phase deformation can be considered based on two foliations, (S_1 and S_2) as well as by inclusion trails in porphyroblasts. D_1 (first deformational phase) is affected by D_2 (second and main deformational phase) with respect to the microscopic thin sections and field evidence. D_2 is the most obvious and pervasive deformation in the area while D_1 can be seen in some thin section, only.
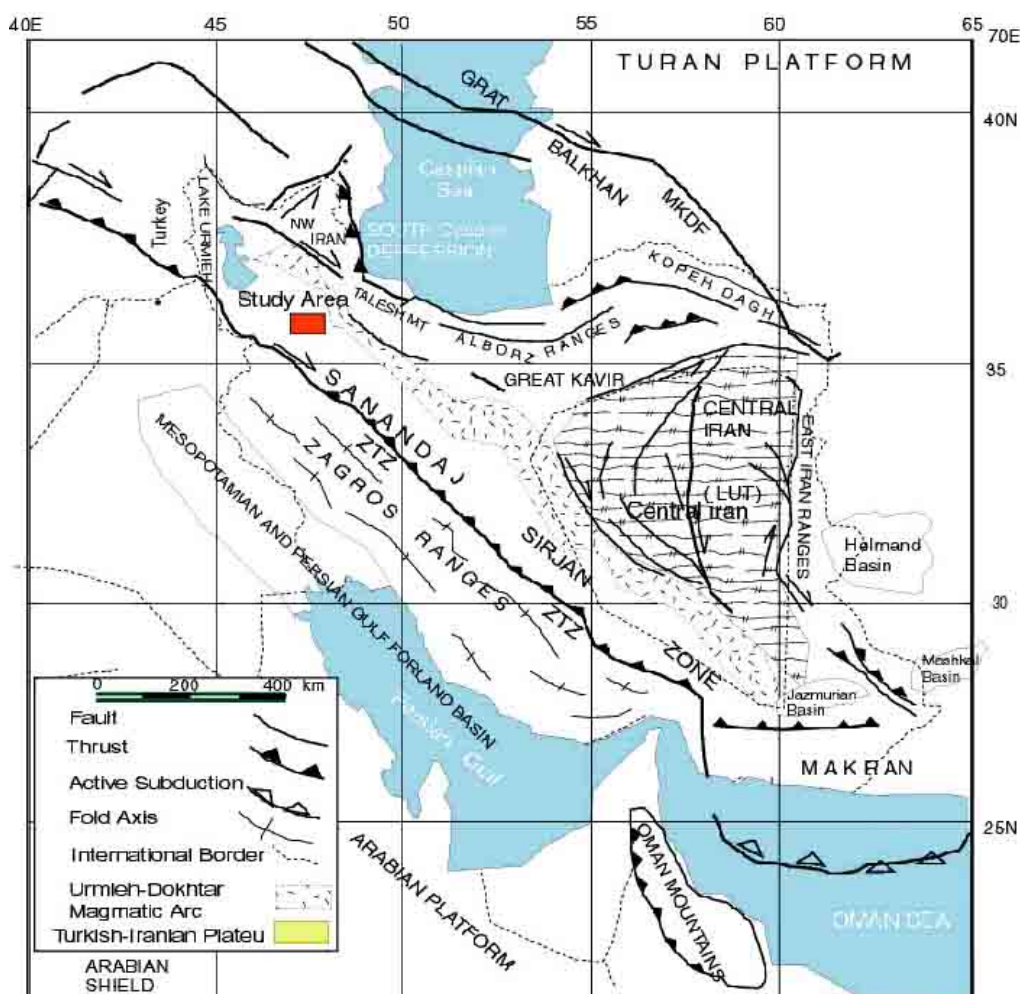

Fig.1. Simplified structural map of Iran (compiled from [3]; [2]). MKDF = Main Kopeh-Dagh Fault, ZTZ = Zagros Thrust Zone.
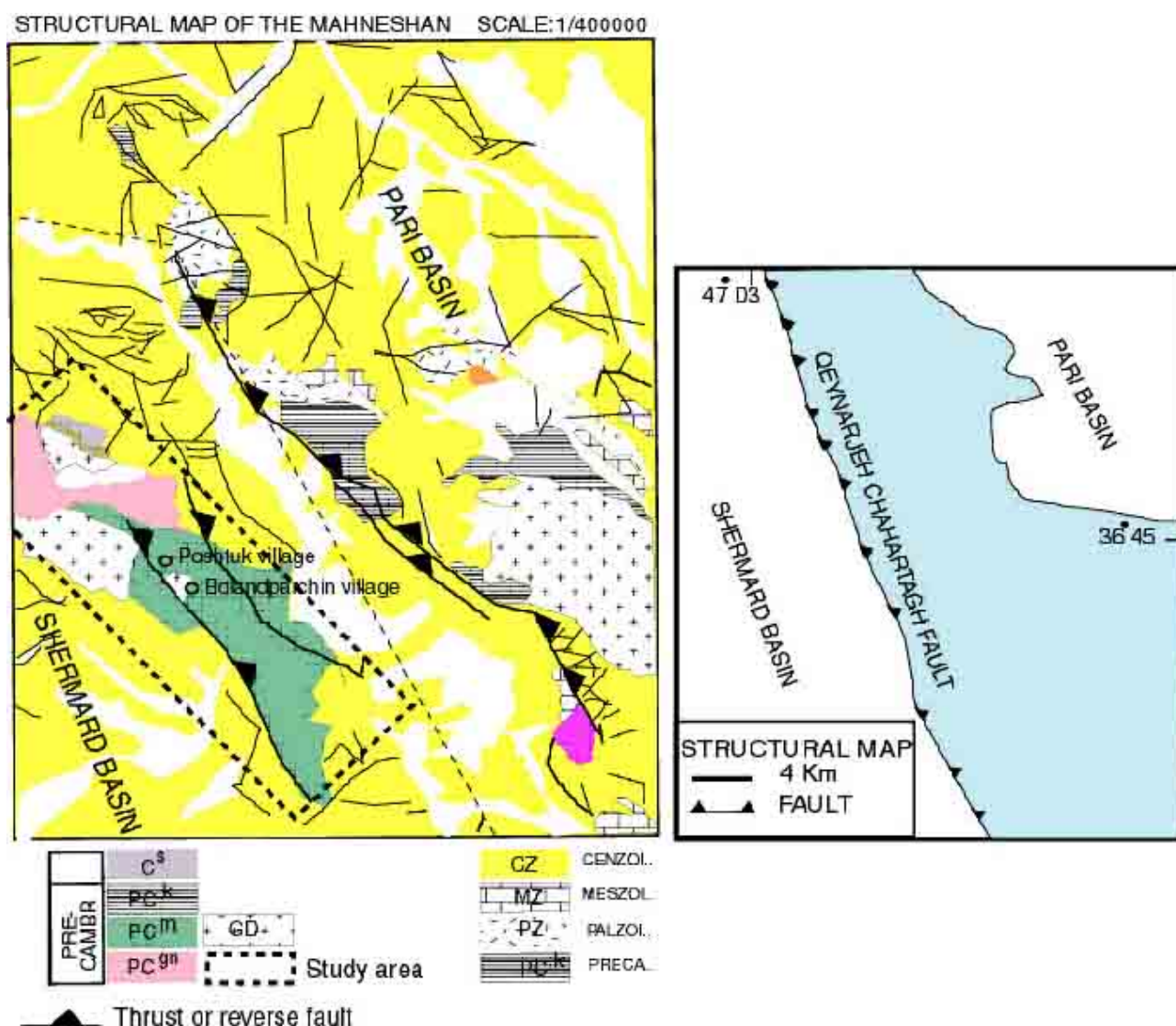
Fig.2. The simplified geological and structural map of the Mahneshsn complex.

3.2. Formation of foliations (S1 and S2)
The slaty cleavage S_1 (formed during the first deformation D_1) is best seen in samples from the Almalu schist where it is brought about by two mica (Bt , Ms) crystallized parallel to the slaty cleavage (Fig. 4c, 5b) and also in crenulation cleavage (Fig 5c). S_2 (formed during the second deformation D_2) is parallel to axial planes of micro-folds in intercalated quartz – feldspar rich and phylosilicate-rich layers. This foliation represents the main regional foliation and can be recognized at all part of the metamorphic zone. S_2 foliation might have developed simultaneously with first generation of the folds and thrusts, superimposed on older structures.

3.3. Relation between deformation and metamorphism (Poly-metamorphism)
a) M1 metamorphism
The M_1 metamorphic phase formed during D_1 deformational phase is represented by fine to medium – grained (0.5-1mm) metamorphic minerals which are present in the weakly-deformed domains. The main minerals of this metamorphic phase (with respect to inclusion in porphyroblast) are garnet, white mica, biotite, chlorite, quartz and albite.

The mica flakes may have grown as crystals parallel to bedding due to diagenetic foliation under low- grade metamorphic condition, simultaneously to the D_1 deformation.

b) M2 metamorphism

The M_2 metamorphic phase is characterized by a strong crenulation cleavage and preferred alignment of mainly mica minerals (S_2) and development of new porphyroblasts including Grt, Bt, Ctd, And, Ky, Sill and St. This phase was the major regional metamorphic phase in the studied area and affected the M_1 metamorphic phase. Name abbreviations are after [6].

Two main mineral assemblages formed during M_2 in the graphitic schists (Bolandparchin sub area Fig.4) and non-graphitic schist (Poshtuk sub area Fig.5).

The graphitic schists assemblages (chloritoid-free) are (in addition to muscovite, quartz as KFMASH system minerals):

Chl + Bt	(1)
Bt + Grt	(2)
Bt + Grt + And + St	(3)
Bt + Grt + And + Ky	(4)
Bt + Grt + Sill	(5)

The mineral assemblages in the non-graphitic schists are

Grt + St + Chl	(6)
Ctd + Grt + St + Chl	(7)

The crystallization of these minerals was found to be temporally related to the S_2 fabric and D_2 phase in all domains.

c) M3 metamorphism

The M_3 metamorphic stage represents a contact metamorphic phase. This metamorphism is affected M_1 and M_2 regional metamorphic phases. Some minerals such as biotite and garnet are replaced the old regional metamorphic garnet due to contact metamorphism. Also and is formed in phyllosilicate-rich layers, over printing both S_1 and S_2 (Fig.4h). The main assemblage of contact metamorphic phase is Grt + Bt + And + Crd + Ms.

d) M4 metamorphism

This metamorphism is retrograde and a post-magmatic event. M_4 metamorphism has affected M_1, M_2 and M_3 metamorphic assemblages, overprinting both S_1 and S_2 schistosities (Fig.4b).

The mineral assemblage that formed during metamorphism ($M_{4)}$, is Chl + Ms. Retrograde reaction textures such as Chl after Bt and Grt are observed mainly in the regional Grt zone and St – And zone.

3.4. Metamorphic mineral growth

a) Chlorite

Primary chlorite is crystallized in the non-graphitic schists. The rocks containing primary chlorite are composed of fine-grained muscovite, chlorite, quartz and porphyroblasts of helsitic garnet and staurolite (Fig.5g). Chlorite and muscovite up to 0.3 mm long have developed in the rocks. Retrograde chlorite is crystallised after both M_1 and M_2 metamorphism (Fig.4b).

b) Biotite

Pelitic rocks from the Alemalu area (Fig.3) are phyllites or fine grained schists with lepidoblastic texture and are characterized by a slaty cleavage, which is affected by later crenulation cleavage. The mineral assemblage of these rocks is Chl + Ms + Bt + Qtz + Pl with opaque accessory minerals (Fig.4c).

c) Garnet

Garnet in the graphitic schists (1 up to 4 mm in diameter) usually forms idioblastic to sub-idioblastic, sometimes inclusion- rich grains with Bt and/or Qtz inclusion. Texture of these schists is lepidoporphyroblastic. Grt, Bt and Ms are syn-tectonic (D_2), because porphyroblasts of Ms and Bt lie parallel to S_2 and wrap garnet (Fig.4f). Garnet predates D_2 deformational phase in some sample (Fig.4e).

Most of the garnet crystals (in non-graphitic schists of Poshtuk) show spiral shape inclusion fabrics, which have traditionally been interpreted as developed during syn-tectonic (S_2) growth of rotating porphyroblasts (Fig5d). Porphyroblasts of garnet up to 1.3 mm long have developed in the non-graphitic schists of the Poshtuk area (Fig.5a).

d) Andalusite

Andalusite exists in the chloritoid-free schists. With respect to the petrography studies, two types of andalusite can be distinguished in graphitic schists:

The first generation of andalusite (And_1) which is formed pre-tectonically to syn-tectonically (D_2) in term of deformation in the crystals, pressure shadow and boudins (Fig.4e). Mica parallel to S_2

wraps the andalusite. And$_1$ is formed during the M$_2$ metamorphic phase. Some of these andalusites have preserved garnet, graphite and staurolite as inclusion and show zoning under the microscope.

The second generation of andalusite (And$_2$) is formed post-tectonically (M$_2$) and due to M$_3$ contact metamorphism. And$_2$ grows statically over pre–existing microfolds of S$_2$ foliations and phylosilicate –rich layers (Fig.4h).

Two textural generations of biotite and garnet can be distinguished.

Mineral growth outlasted the deformation, as indicated by And$_2$, Grt$_2$ and Bt$_2$, porphyroblasts either growing statically over pre–existing microfolds of S$_2$ or replacing a former mineral that formed during regional metamorphism such as Grt$_1$.

e) Staurolite

Staurolite is crystallized in both chloritoid-free and chloritoid-bearing schists. There is no pressure shadow around this mineral. It seems that the staurolites are syn-D$_2$ (Fig.4h). S$_2$ schistosity wraps some staurolites. Staurolite usually forms idioblastic to sub-idioblastic, inclusion- free grains. Staurolite in chloritoid-bearing schists of Poshtuk often nucleated at the margin of garnet or in phyllosilicate – rich layers (Fig.5.e). Most of the garnet has already broken down in these rocks and staurolite is formed at the rim of garnet (Fig.5.f).

f) Chloritoid

Chloritoid was found in non-graphitic schists in the study area. It occurs in fine-grained rock matrix as lath-shaped crystals with bluish colour under the microscope (Fig.5g). These rocks consist of garnet (up to 1.3 mm) chloritoid, staurolite (up to 0.5 mm), chlorite and muscovite. Chloritoid, chlorite and muscovite are formed parallel to S$_2$ in non-graphitic schist that wraps spiral garnet. These minerals are syn- D$_2$. Therefore main mineral assemblage in these rocks, which are formed syn-M$_2$, is: Ctd + Grt + St + Ms + Chl + Qtz.
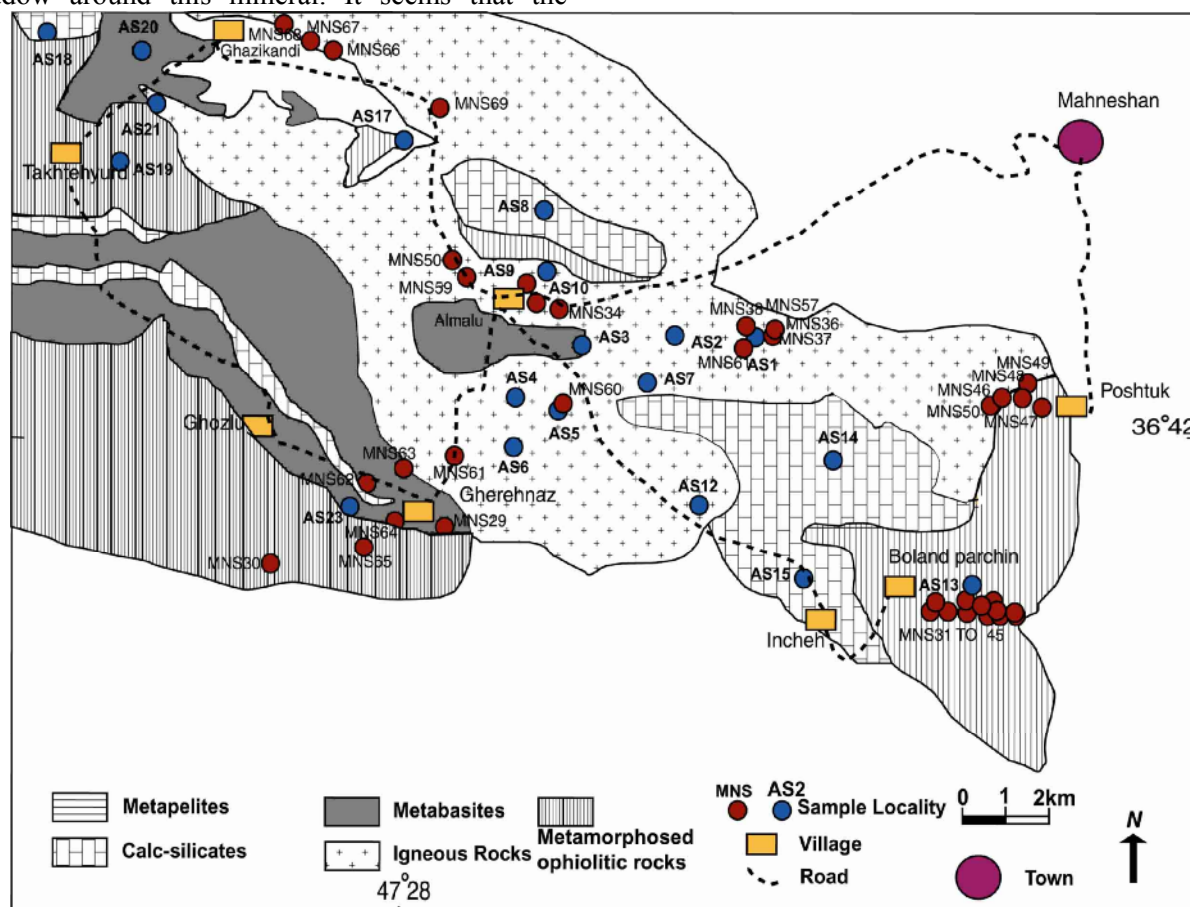

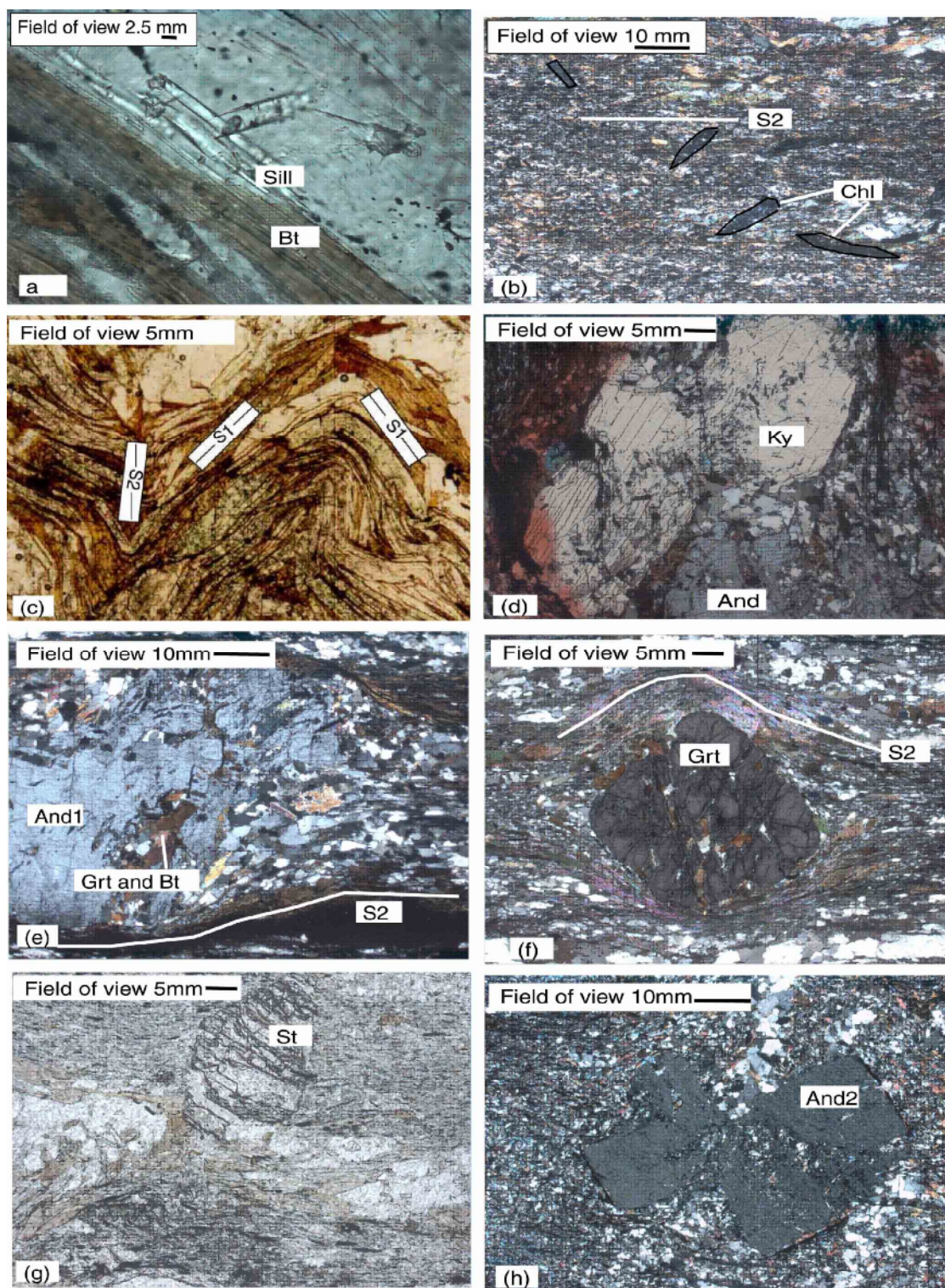**Fig.3.** Geological map of the Mahneshan Complex whit sample locations [25].

Fig. 4. a- sillimanite grows at the expense of biotite. b- Retrograde chlorite over printing both S_1 and S_2 foliation. c- A schistosity (S_1) is defined by a preferred orientation of muscovite, and biotite affected by a crenulation schistosity with an axial plane cleavage (S_2) defined by Bt and Ms. d- Kayanite porphyroblast formed during M_2 regional metamorphism. e- Syn-tectonically andalusite (And_1) and deformed porphyroblast formed during M_2 main regional metamorphism and deformed S_2 foliation with rotated andalusite porphyroblast. f- Syn-tectonic garnet porphyroblasts formed during M_2 metamorphism. g- Staurolite is formed syn-tectonically in the chloritoid-free schists. h- Undeformed andalusite (And_2) porphyroblast has overgrown D_2 micro fold during M_3 contact metamorphism.
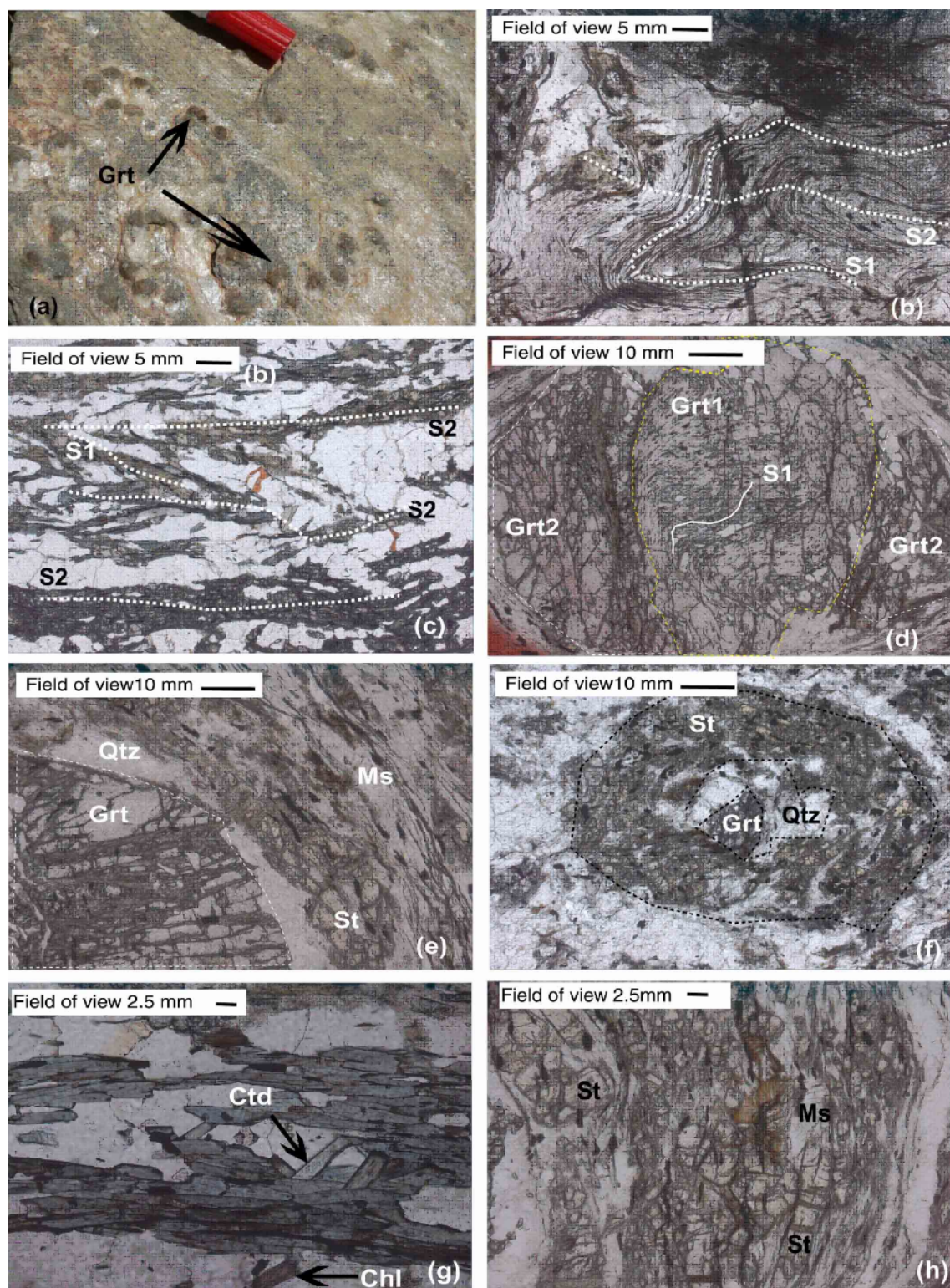
Fig. 5. a. garnet porphyroblasts (Grt) with 0.5 to 1.5 cm diameter formed in chloritoid schists. b. folding of the S1 foliation leading to the development of a S2 foliation parallel to the axial plane. c. A schistosity (S$_1$) is defined by a preferred orientation of muscovite, chloritoid and chlorite which is crenulated. d. Syn-tectonic helcitic garnet porphyroblasts(Grt$_1$) formed during M$_2$ metamorphism and garnt (Grt2)is formed during contact metamorphic phase. e. Staurolite and muscovite nucleated at the margin of garnet. f. garnet (pseudomorph) is replaced by staurolite (prograde metamorphism). g. Chlorite and chloritoid in textural equilibrium. h. staurolite pseudomorphed by muscovite

g) Sillimanite

Pelitic rocks of Bolandparchin, which contain sillimanite, are medium – grained schists (Fig.4a). Sillimanite aggregates are associated with biotite and also are in contact with andalusite. The typical assemblage (in addition to muscovite + quartz + plagioclase) is Bt + Grt + And + Sill with minor Fe – Ti oxides.

4. Mineral chemistry of peak metamorphism

In order to identify the mineral composition of major phases of metapelites in the studied samples, minerals in five representative thin sections of the rocks were analysed with the electron microprobe in GeoForschungsZentrum (GFZ) Potsdam, Germany, using a CAMECA model SX100 microprobe in the wavelength-dispersive mode with 15 Kv acceleration Voltage, 3 nA beam current and 40 second acquisition time per analyses. The detection limit of the machine is approximately 0.1 wt%. The relative analytical errors are approximately 1%.

Sample locations are shown in Figure 3. Representative mineral analyses are provided in Tables 1, 2 and 3.

Table 1. Representative Chlorite and muscovite analyses and the structural formulae

Sampel	13f	13b	13a	49g	49g	43b1	43b1	43c	43c	44c	44c	13f	13a	13b
Mineral	Chl	Chl	Chl	Chl	Chl	Ms	Ms	Ms	Ms	Ms	Ms	Ms	Ms	Ms
								Pre	Pre	Post				
SiO$_2$	23.62	23.83	23.53	23.29	23.90	46.10	45.85	44.73	46.63	46.34	46.54	47.21	47.12	46.48
TiO$_2$	0.07	0.09	0.09	0.12	0.52	0.28	0..33	0.47	0.44	0.70	0.54	0.29	0.29	0.28
Al$_2$O$_3$	22.76	22.74	22.77	23.25	21.66	38.52	38.43	34.90	36.30	36.70	37.68	35.38	35.51	35.26
Cr$_2$O$_3$	0.00	0.00	0.00	0.11	0.06	0.03	0.07	0.04	0.05	0.03	0.01	0.00	0.00	0.00
Fe$_2$O$_3$	0.00	0.00	0.00	1.11	0.00	0.73	0.88	3.40	0.92	0.86	1.00	0.00	0.00	0.00
FeO	28.77	28.42	28.70	32.96	37.95	0.16	0.20	0.76	0.21	0.19	0.22	1.00	0.79	0.86
MnO	0.38	0.42	0.27	0.02	0.06	0.00	0.02	0.01	0.03	0.00	0.00	0.00	0.01	0.01
MgO	11.68	11.71	11.44	8.58	5.07	0.36	0.37	1.17	0.58	0.60	0.68	0.67	0.55	0.61
CaO	0.00	0.02	0.05	0.00	0.01	0.01	0.00	0.01	0.00	0.00	0.01	0.00	0.20	0.05
Na$_2$O	0.00	0.00	0.02	0.00	0.01	1.72	1.62	0.79	1.20	1.00	0.97	1.02	0.79	0.98
K$_2$O	0.00	0.05	0.00	0.00	0.25	8.81	9.17	9.05	9.70	10.00	10.02	9.21	8.41	8.87
Totals	87.30	87.28	86.87	89.00	89.49	96.73	96.95	95.00	96.00	96.40	97.00	94.87	93.81	93.44
	(O) 28							11 (O)						
Si	2.55	2.57	2.55	2.48	2.61	2.99	2.98	2.98	3.00	3.03	3.00	3.12	3.13	3.11
Ti	0.07	0.00	0.00	0.01	0.043	0.01	0.02	0.02	0.02	0.03	0.026	0.01	0.01	0.01
Al	2.76	2.90	2.92	2.92	2.80	2.946	2.94	2.74	2.90	2.83	2.87	2.75	2.78	2.78
Cr	0.00	0.00	0.00	0.00	0.00	0.00	0.00	0.00	0.00	0.00	0.00	0.00	0.00	0.00
Fe(3+)	0.00	0.00	0.00	0.09	0.00	0.01	0.01	0.17	0.04	0.04	0.05	0.04	0.03	0.40
Fe(2+)	2.60	2.57	2.60	3.12	3.65	0.009	0.02	0.04	0.01	0.01	0.01	0.01	0.00	0.01
Mn	0.03	0.04	0.02	0.00	0.00	0.00	0.00	0.00	0.00	0.00	0.00	0.00	0.00	0.00
Mg	1.88	1.88	1.85	1.36	0.825	0.03	0.03	0.11	0.05	0.06	0.06	0.06	0.05	0.06
Ca	0.00	0.00	0.00	0.00	0.00	0.00	0.00	0.00	0.00	0.00	0.00	0.00	0.01	0.00
Na	0.00	0.00	0.00	0.00	0.002	0.216	0.20	0.10	0.15	0.12	0.12	0.13	0.10	0.12
K	0.00	0.00	0.00	0.00	0.035	0.730	0.76	0.77	0.80	0.83	0.83	0.77	0.71	0.75
Totals	9.98	9.97	9.98	10	9.967	6.91	6.90	6.90	6.98	6.97	6.98	6.92	6.85	6.90

Table 2. Representative biotite and garnet analyses and the structural formulae.

Mineral	43c	43c	44c	44c	13b	43b1	43b1	44c	44c	44c	43b1	43b1	44c
	Bt	Bt	Bt	Bt	Bt	Bt	Bt	Grt	Grt	Grt	Grt	Grt	Grt
Sample	Post	Post	Pre	Post		Syn	Post	Rim	Post	Core	Core	Rim	Core
SiO2	34.95	35.25	40.73	34.40	34.34	35.62	34.36	36.8	36.50	37.11	38.11	35.02	36.50
TiO2	1.96	2.05	1.55	2.45	1.36	1.57	1.62	0.04	0.05	0.00	0.00	0.02	0.02
Al2O3	20.15	20.80	28.52	20.23	19.66	20.32	19.54	21.07	20.95	21.30	20.67	19.98	20.60
Cr2O3	0.01	0.03	0.04	0.00	0.00	0.00	0.00	0.03	0.01	0.01	0.01	0.01	0.00
Fe2O3	0.00	0.00	0.00	0.00	0.00	0.00	0.00	1.93	2.23	1.90	1.80	1.10	1.61
FeO	22.93	21.77	11.18	21.85	21.84	19.89	21.74	28.44	31.64	31.26	30.00	30.05	30.72
MnO	0.17	0.11	0.05	0.24	0.20	0.12	0.12	8.25	5.86	5.84	8.18	8.09	6.09
MgO	8.43	8.60	4.50	8.58	7.82	8.74	8.85	1.80	2.28	2.63	1.41	1.88	2.50
CaO	0.02	0.00	0.03	0.01	0.12	0.15	0.33	3.18	1.60	1.96	2.55	1.38	1.81
Na2O	0.19	0.32	0.13	0.12	0.32	0.08	0.14	0.00	0.00	0.00	0.00	0.00	0.00
K2O	8.91	9.06	6.40	8.05	8.11	8.43	7.35	0.00	0.00	0.00	0.00	0.00	0.00
Totals	97.00	97.90	93.13	95.50	94.07	94.93	94.06	101.5	101.13	101.9	102	101	99.85
	11 (O)							12 (O)					
Si	2.62	2.62	2.90	2.61	2.67	2.70	2.65	2.94	2.93	2.94	3.027	2.94	2.96
Ti	0.11	0.11	0.08	0.14	0.08	0.09	0.09	0.00	0.00	0.00	0.00	0.00	0.00
Al	1.78	1.82	2.40	1.81	1.80	1.81	1.78	2.00	2.00	2.00	1.935	2.00	1.97
Cr	0.00	0.00	0.00	0.00	0.00	0.00	0.00	0.00	0.00	0.00	0.00	0.00	0.00
Fe(3+)	0.00	0.00	0.00	0.00	0.00	0.00	0.00	0.11	0.13	0.14	0.107	0.09	0.10

Fe(2+)	1.44	1.35	0.66	1.39	1.42	1.26	1.40	1.90	2.13	2.07	2.09	2.09	2.08
Mn	0.01	0.00	0.00	0.01	0.01	0.00	0.00	0.55	0.40	0.393	0.55	0.50	0.41
Mg	0.94	0.95	0.47	0.97	0.90	0.99	1.02	0.21	0.27	0.311	0.167	0.235	0.30
Ca	0.00	0.00	0.00	0.00	0.01	0.01	0.03	0.27	0.14	0.167	0.217	0.17	0.15
Na	0.02	0.04	0.01	0.02	0.05	0.01	0.02	0.00	0.00	0.00	0.00	0.00	0.00
K	0.85	0.85	0.48	0.78	0.80	0.82	0.72	0.00	0.00	0.00	0.00	0.00	0.00
Totals	7.70	7.78	7.12	7.74	7.77	7.71	7.73	8.05	8.00	8.00	8.05	7.87	8.00

Table 3. Representative staurolite, chloritoid and plagioclase analyses and the structural formulae

Mineral	St	St	St	St	St	St	St	Ctd	Ctd	Ctd	Pl	Pl	Pl
	Inc	Inc	Core	Core	Rim	Rim	Core	Core	Core				
Sample	43c	43c	49g	13b	13b	13a	13a	49g	49g	49g	44c	44c	13f
SiO2	27.00	26.04	27.45	27.28	25.87	25.66	25.47	24.60	24.44	24.45	60.61	60.70	63.42
TiO2	0.55	0.45	0.52	0.31	0.35	0.30	0.31	0.00	0.02	0.01	0.00	0.00	0.01
Al2O3	55.60	57.34	57.14	53.60	54.36	54.83	54.82	41.35	41.26	41.10	26.22	26.11	22.92
Cr2O3	0.04	0.07	0.04	0.00	0.00	0.00	0.00	0.07	0.06	0.04	0.00	0.00	0.00
Fe2O3	0.00	0.00	0.00	0.00	0.00	0.00	0.00	1.31	2.10	1.30	0.04	0.07	2.40
FeO	13.57	11.90	14.24	14.00	13.80	14.26	14.30	26.37	26.16	26.41	0.00	0.00	0.01
MnO	0.36	0.28	0.07	0.60	0.60	0.40	0.40	0.03	0.00	1.01	0.00	0.00	0.15
MgO	1.45	1.01	0.32	1.22	1.06	1.16	1.21	1.65	1.70	1.65	0.00	0.00	0.04
CaO	0.01	0.01	0.00	0.00	0.00	0.00	0.00	0.01	0.02	0.00	6.77	6.75	2.40
Na2O	0.05	0.05	0.00	0.01	0.00	0.03	0.01	0.00	0.01	0.00	8.46	8.53	7..91
K2O	0.01	0.01	0.01	0.00	0.00	0.00	0.00	0.02	0.00	0.01	0.12	0.10	2.04
Totals	98.00	97.00	99.00	97.00	96.02	96.64	96.52	95.41	95.76	95.10	101.9	102	98.93
	23 (O)							12 (O)			8 (O)		
Si	7.43	7.20	7.46	7.66	7.34	7.25	7.21	0.994	0.986	0.997	2.65	2.66	2.83
Ti	0.11	0.09	0.106	0.06	0.07	0.06	0.06	0.00	0.00	0.00	0.00	0.00	0.00
Al	18.04	18.70	18.31	17.73	18.20	18.27	18.30	1.97	1.96	1.96	1.35	1.34	1.21
Cr	0.00	0.01	0.00	0.00	0.00	0.00	0.00	0.00	0.00	0.00	0.00	0.00	0.00
Fe(3+)	0.00	0.00	0.00	0.00	0.00	0.00	0.00	0.04	0.06	0.04	0.00	0.00	0.00
Fe(2+)	3.12	2.75	3.23	3.30	3.27	3.37	3.38	0.89	0.88	0.90	0.00	0.00	0.01
Mn	0.08	0.06	0.016	0.14	0.14	0.09	0.09	0.00	0.00	0.00	0.00	0.00	0.00
Mg	0.60	0.41	0.13	0.51	0.45	0.50	0.51	0.10	0.10	0.10	0.00	0.00	0.00
Ca	0.00	0.00	0.00	0.00	0.00	0.00	0.00	0.00	0.00	0.00	0.32	0.32	0.11
Na	0.02	0.02	0.00	0.00	0.00	0.01	0.00	0.00	0.00	0.00	0.72	0.74	0.68
K	0.00	0.00	0.00	0.00	0.00	0.00	0.00	0.001	0.00	0.00	0.00	0.00	0.12
Totals	29.43	29	29.27	29.40	29.48	29.55	29.57	4.00	4.00	4.00	5.0.4	5.04	4.96

a) Chlorite

Representative analyses of chlorite are shown in Table 1. The number of cations is calculated on the basis of 28 Oxygens. Prograde chlorite is only present in non-graphitic schists. Retrograde chlorite, formed as alteration product of biotite and garnet has almost the same composition as the prograde ones. The oxide totals are between 86.87 and 89.49. The amount of Ti is between 0.01 and 0.07 atom per formula unit (apfu). The chlorites are Mn-free. Na varies from 0.00 to 0.02 apfu, and K from 0.00 to 0.03 apfu. Substitution of Al^{3+} for Si^{4+} is calculated using stoichiometric approach. Figure 6a after [7] shows the classification of the studied chlorites. According to this figure, chlorites are of ripidolite to daphnite type. This figure also shows the Fe-rich nature of the chlorites. According to Fig. 6b [8] retrograde chlorites plot on the Medium-/Low-pressure field and prograde chlorite plot close to this field.

b) Muscovite

Muscovite analyses are listed in Table 1. The number of cations is calculated on the basis of 11 oxygens. All samples of pelitic composition contain primary muscovite. There is no compositional difference between those lying parallel to the schistosity and those oblique to the S_2 foliation. According to Figure 6c [9], muscovite is rich in the muscovite end-member Figure 6d, paragonite being the second dominant component. The mole fractions of other components are negligible. Reduction in the phengite component of muscovite with metamorphic grade has been described by several authors (e.g. [10]; [11]; [12]) in different low-to medium pressure metamorphic terranes.

c) Biotite

Microprobe analyses of biotite are provided in Table 2. The number of cations is calculated on the basis of 11 oxygens. The amount of Ti is between 0.08 and 0.14 (apfu). Phlogopite-annite are the dominant constituents in the biotite (Fig.6d1). Ti versus Fe/(Fe+Mg) diagram for biotites from different metamorphic zones, is given in Figure 6e. Compositional ranges of biotite from various metamorphic zones in New England are from [13].

According to this figure, biotites in the studied samples plot in the Ky-St and Sil-St zones. This is in accordance with petrographical observation.

d) Garnet
Garnet compositions are listed in Table 2. In general, garnets are Fe-rich with almandine content varying between 80 and 90 %. Ti is not presented or occurs in very low amounts. Figure 6g shows

the chemical composition of the analysed garnets on the Alm, Pyp and (Grs+Sps) triangular diagram. Fe^{3+} content of g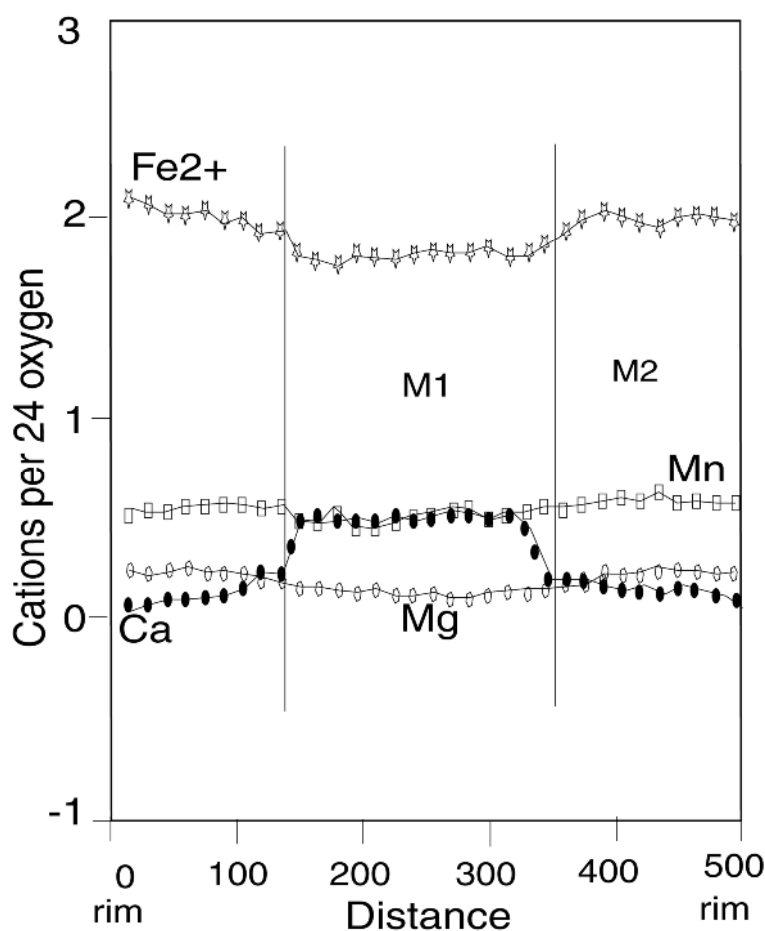arnet were calculated based on eight cations and 12 Oxegens. Zoning profiles are from rim to rim through the core of the garnets (Fig 6k). There is significant normal zoning in the garnet from sample 43b1.
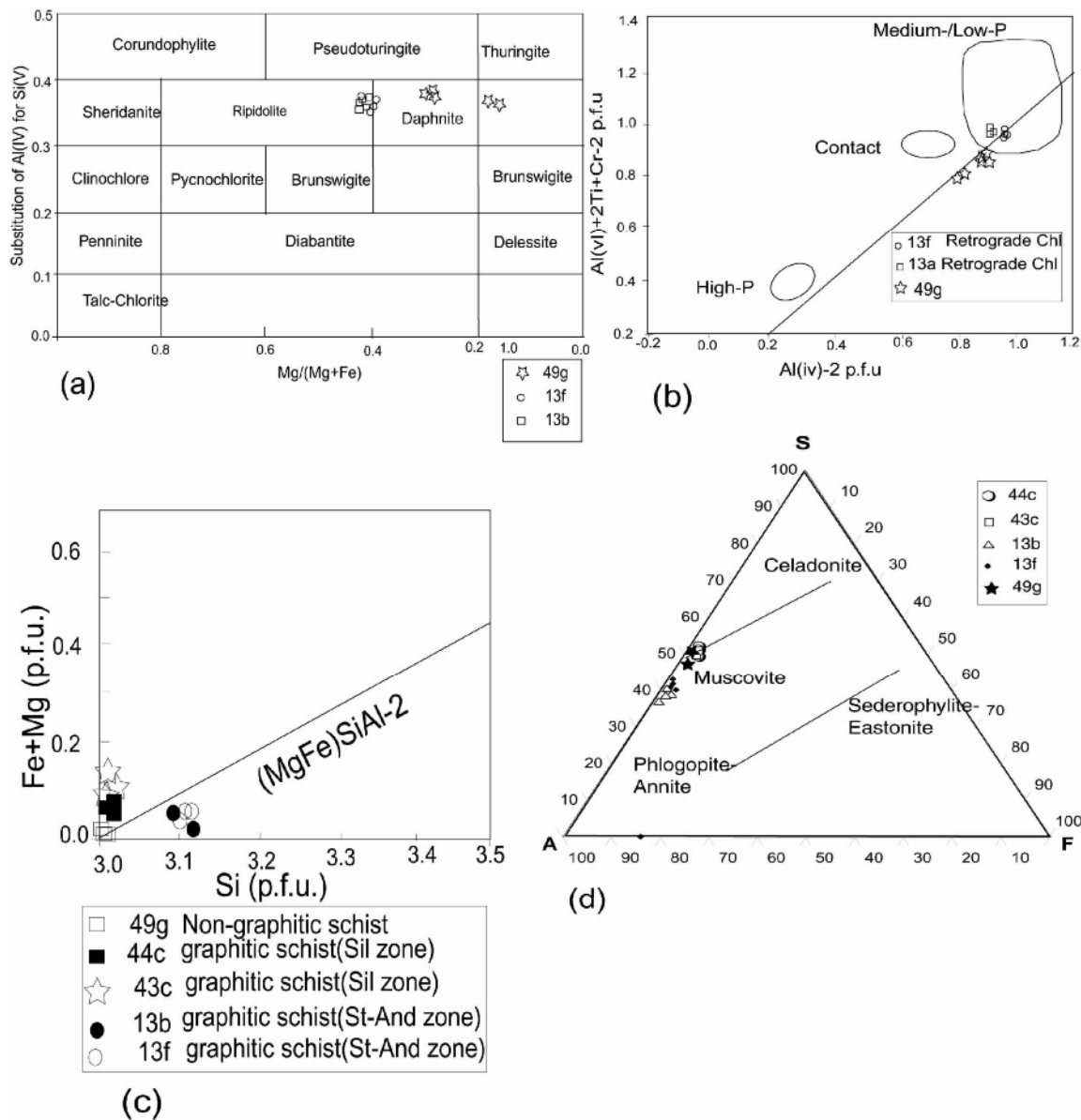
Fig. 6. a. Classification of the analysed chlorites using Al^{3+} substitution for Si^{4+} versus $Mg/(Mg+Fe^{2+})$ diagram. Chlorites in all samples are ripidolite to daphnite in composition. b. Chlorite composition of Mahneshan metapelite on a formula proportion diagram (Al(VI)+2Ti+Cr-2 versus Al(IV)-2). Compositional variation along the 1:1 line represents the Tschermak substitution. Indicated field for different metamorphic condation after [8]. c. Chemical compositions of muscovites from metapelits of Mahneshan. Si (Per 11 oxygens) against Fe+Mg.
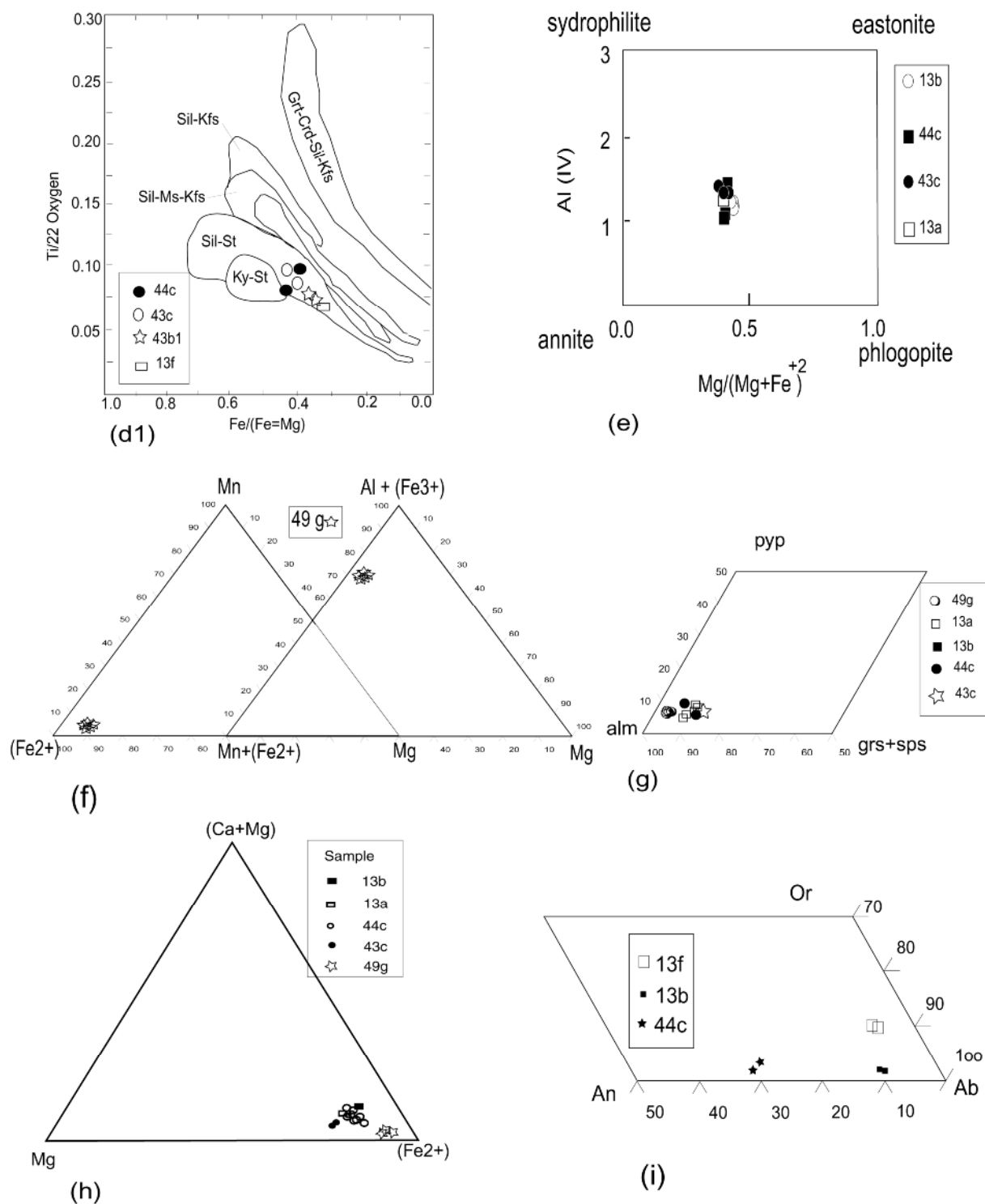
Fig. 6. d1. Plot of Ti (per 11 oxygens) as a function of Fe/(Fe+Mg) for biotite from different metamorphic zones. 5.e.Unshaded fields: compositional ranges of biotite from metapelites of Mahneshan ([13]). f. Composition of the studied chloritoids plotted on the Mn, Fe^{2+}, Mg and Fe^{2+} + Mn, Al+Fe^{3+}, Mg triangular diagrams. Chloritoids are Fe-chloritoid. g. Composition of the studied garnet plotted on the Fe^{2+}, Mg and Ca, triangular diagrams. h. Composition of the studied staurolite plotted on the Fe^{2+}, Mg and Mn + Ca triangular diagrams. i. Composition of the Mahneshan igneous feldspars, plotted on the An-Ab-Or diagram.

Fig. 6. k. Zoning profiles from rim to rim through the core of the garnets. There is significant normal zoning in garnet from sample 43b1.

e) Chloritoid

Chloritoid is found only in Non-graphitic schists. Representative mineral compositions of chloritoids in the studied samples are given in Table 3. The number of cations is calculated on the basis of 12 Oxygens. Chloritoids are iron rich, and the Fe/Mg ratio is much higher than in the coexisting chlorite. Fig.6f, illustrates the composition of chloritoids on the $Al+Fe^{3+}$, $Fe^{2+}+Mn$, Mg and Fe^{2+}, Mn, Mg triangular diagrams. According to the figure, Fe^{2+} occupies the cubic site (i.e. chloritoids are Fe-rich).

f) Staurolite

Staurolite analyses are listed in Table 3. The number of cations is calculated on the basis of 22 Oxygens. Staurolite in sample 49g, which is associated with chloritoid, has distinctly less MgO (~0.35%) and ZnO(~0.30 %) than staurolite in

sample 43c associated with andalusite and/or kyanite, with MgO(~1.22%) and ZnO((~1.78 %). Staurolite do not show any significant zoning. Fig.6h, shows compositional ranges of staurolite on the Fe, Mg and (Mn+Zn) triangular diagrams. According to the figure, staurolites are Fe-staurolite and MnO and ZnO contents are very low. Staurolite shows lower X_{Fe}-value than coexisting garnet.

g) Feldspar

Feldspar analyses are listed in Table 3. The number of cations is calculated on the basis of 8 Oxygens. The anorthite content (XAn) of plagioclase is variable. For example in sample 44c XAn is 0.30 and in sample13f it is 0.10. Figure 6i, illustrates the composition of feldspars on the Ca,

Na, K triangular diagram. According to the figure, plagioclases are albite-rich.

5- Discussion

5-1- Phase relation and reaction history of peak
metamorphism (M_2) in the chloritoid-free metapelitic rocks of the Bolandparchin sub-area
AFM compatibility diagrams, constructed based on real minerals chemistry, show phase relation for the garnet zone to sillimanite zone in the chloritoid-free metapelites (Fig.7).

a) The biotite-in isograd
The initial assemblege in the graphitic metapelitic rocks of the Bolandparchin sub area was probably, Kfs (detrital) + Chl + Ms + Qtz.

At the biotite-in isograd the first appearance of biotite in these rocks could be resulted from a KFMASH continuous reaction, such as

$$Kfs + Chl = Bt + Ms + Qtz + H_2O \qquad (1)$$

The appearance of biotite in semi-pelitic rocks with detrital K-feldspar can be explained by this reaction.

Reaction (1) is also proposed by [10] for pelitic rocks from the Scottish Dalradian. We adopt the generally assumed temperature for the biotite in isograd of 370-400°C.

Bucher and Frey [14] discuss the eqilibrium condition of such a reaction as a function of X_{FeO}. The pelites lacking K-feldspar, dominate the metasedimentry sequence. In these rocks biotite forms most probably by the continuous reaction

$$Phe + Chl = Bt + Phe\text{-poor } Ms + Qtz + H_2O \qquad (2)$$

According to Bucher and Frey [14] this reaction involves the progressive replacement of chlorite and the reduction of the phengite component in muscovite.
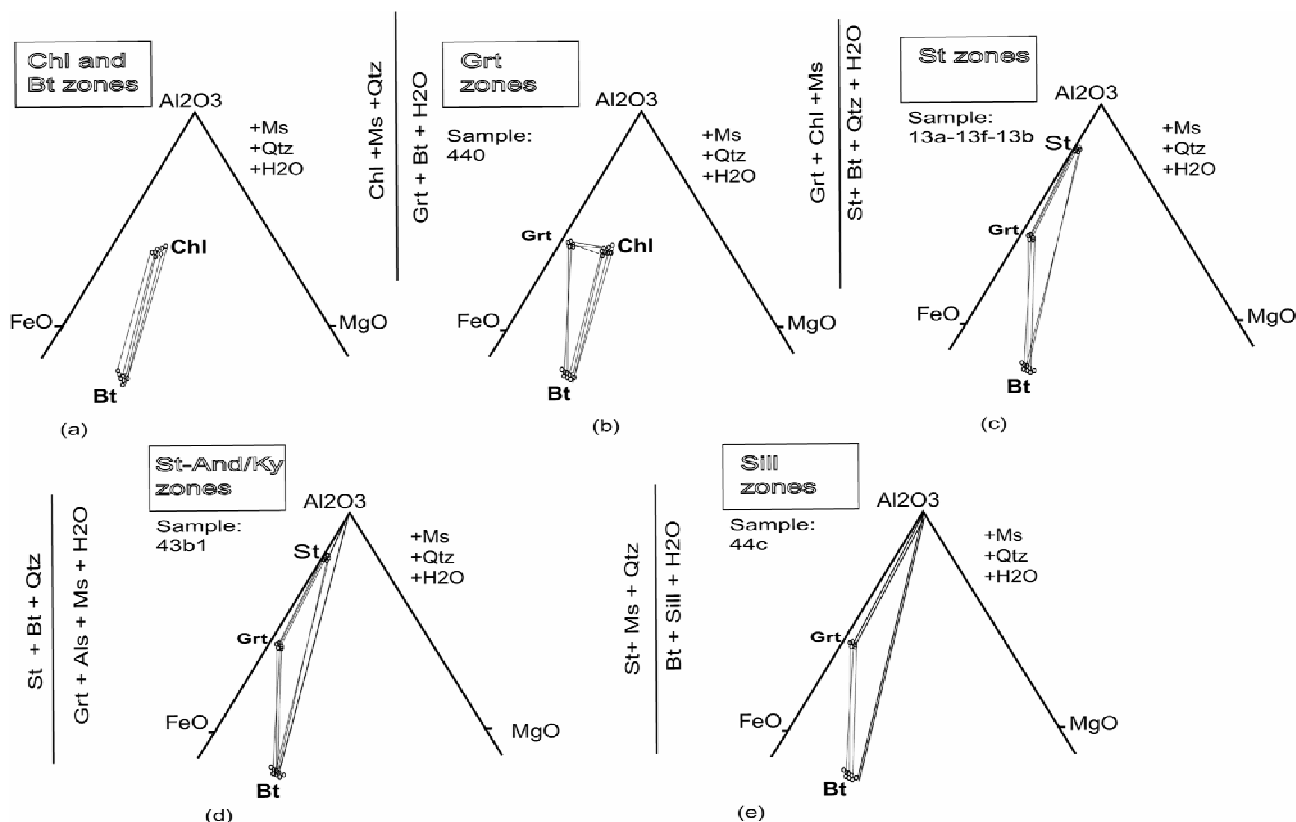

Fig. 7. a to e, Al_2O_3-FeO-MgO projection from quartz, muscovite and H_2O for coexisting minerals in graphitic schists of the Bolandparchin sub-area.

b) The garnet-in isograd

The garnet-in isograd reaction is strongly depended on bulk-rock composition and MnO and CaO contents in the rocks. With high amount of these components, garnet could appear at temperatures below 450°C [15].

The appearance of garnet in the studied graphitic schists is most probably related to the two continuous reactions deduced from the AFM-phase compatibility diagrams (Fig.7 a to e)

$$Chl + Qtz = Grt + H_2O \quad e.g.[16] \qquad (3)$$
$$Chl + Ms + Qtz = Grt + Bt + H_2O \qquad (4)$$
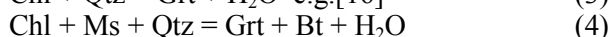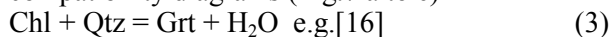
In Bolandparchin sub-area chloritoid dose not occur, due to the MnO content of garnet, which produces an expansion of the Grt-Chl stability field to lower temperatures or to Al-poor bulk composition that contain Grt + Chl assemblages rather than chloritoid + biotite [17]

c) The staurolite-Al2SiO5- in isograd

Staurolite is crystallized in both chloritoid-bearing and chloritoid-free rocks. Staurolite in the chloritoid-free, rocks could have been produced by the following discontinuous reaction.

$$Grt + MS + Chl = St + Bt + Qtz + H_2O \ [18] \qquad (7)$$
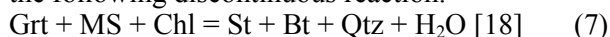
Garnet is partially resorbed by this reaction, and a significant amount of chlorite is removed, along with the production of abundant staurolite and new biotite.

According to [19], this reaction takes place at a fixed temperature for any given pressure, because it is discontinuous and proceeds until one of the three reactants has been consumed. When this reaction ceases, additional staurolite may be produced by a continuous reaction involving the remaining phase, for example

$$MS + Chl = St + Bt + Qtz + H_2O \qquad (8)$$
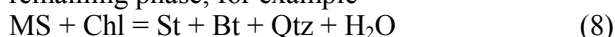
This reaction may be deduced from AFM phase compatibilities and metamorphic textures, in that staurolites occurs mainly in phyllosilicates-rich layers [e.g.20]. These reactions account for the disappearance of primary chlorite in the staurolite-andalusite zone.
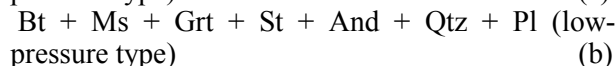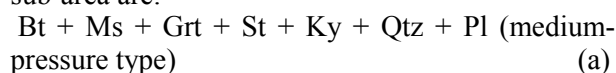
Staurolite dos not appear in samples 13f and 44c (And +Grt + Bt + Ms) but exists as inclusions in andalusite, therefore, the following reaction can be considered for staurolite breakdown:

$$St + Ms + Qtz = Bt + And/Ky + H_2O \qquad (9)$$
$$St + Bt + Qtz = Grt + Als + Ms + H_2O \qquad (10)$$
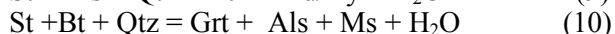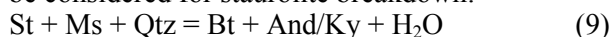
The low pressure andalusite-bearing rocks are mainly exposed in the Bolandparchin area. The appearance of andalusite is most probably related to the reactions

$$Chl + Ms = And + Bt + H_2O \qquad (12)$$

$$Chl + Ms = ky + Bt + H_2O \qquad (13)$$
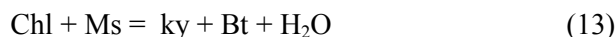
Reaction (12) generally occurs at low-pressure of the lower amphibolite facies, whereas reaction (13) occurs at medium-pressure of the lower amphibolite facies [5]. Two representative mineral assemblages formed during M2 metamorphic phase in the graphitic schists of the Bolandparchin sub-area are:

$$Bt + Ms + Grt + St + Ky + Qtz + Pl \ (medium\text{-}pressure \ type) \qquad (a)$$
$$Bt + Ms + Grt + St + And + Qtz + Pl \ (low\text{-}pressure \ type) \qquad (b)$$

d) The Sillimanite-in isograd

Sillimanite occurs as two types (i) aggregates of fibrolite, overgrowing biotite and muscovite (Fig.4p) (ii) prismatic sillimanite.

The fine- grained fibrolite may have resulted from the following reactions:

$$2Ms + 2H^+ = 3Sil + 3Qtz + 2K^+ + 3H_2O \qquad (9)$$
$$4Bt = 2Sil + 10Qtz + 12(Mg,Fe)O + 2K_2O + 4H_2O \qquad (10)$$
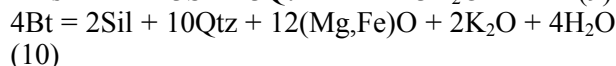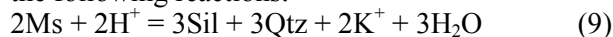
According to Carmichael [18], the development of fibrolite at the expense of micas may be related to a series of local metasomatic cation-exchang reactions.

Staurolite does not appear in this zone, it is preserved as inclusions in andalusite. It may disappear as a result of the discontinuous reaction (11) or continuous reaction (12):

$$St + Ms + Qtz = Sil + Grt + Bt + H_2O \qquad (11)$$
$$St + Ms + Qtz = Al_2SiO_5 + Bt + H_2O \qquad (12)$$
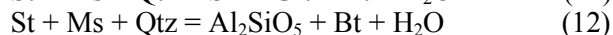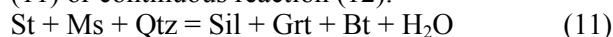
Reaction (12) reflects lower temperature than the discontinuous reaction (11) and P-T condition is nearly independent of the CaO and MnO content of the rock [21].

5-2- Phase relations and mineral reactions in the chloritoid metapelitic rocks of the Poshtuk sub-area

Sample 49g contains the assemblage garnet, staurolite, chlorite, muscovite, chloritoid, quartz. The isograds are not typical Barrovian isograds, but reflect the first appearance of chloritoid in these aluminous bulk compositions. Staurolite does not co-exist with biotite as it does in the classical Barrovian staurolite zone. Petrographical studies of the samples show obvious reaction rims around the garnet crystals.

a) The garnet-in isograd

Chloritoid is formed in non-graphitic schists of the Poshtuk sub-area, Chloritoid acts as a possible reactant for garnet formation in these rocks. This is

deduced from the AFM-phase compatibilities (Fig.8a, b, c)

$$Ctd + Chl + Qtz = Grt + H_2O \text{ [22]} \qquad (5)$$

Fe-chloritoid + annite = almandine + muscovite + H_2O

b) The Staurolit -in isograd

In the chloritoid schists (non-graphitic rocks), textural relations show the formation of staurolite at the expense of garnet (Fig.5) suggesting the following reaction

$$Ctd = St + Grt (Alm) + Chl + H_2O \text{ [23]} \qquad (11)$$

The appearance of staurolite in sample 49g is the result of the continuous Fe–Mg–Mn reaction. The garnet in the garnet zone samples occurs as an extra phase, stabilized by Mn [e.g. 24] (Fig.8d, e, f, g). In the AFM system, the garnet zone samples at a given temperature (T_1) are characterized by co-existing chlorite and chloritoid. At higher metamorphic temperatures (T_2), the reaction:

chloritoid = garnet + staurolite + chlorite, results in the demise of chloritoid in the higher grade rocks and the appearance of staurolite and continued garnet growth. These garnet-bearing rocks are better illustrated in the AFMn system when projected from chlorite. The stable garnet zone (T_1) sub-assemblage is chloritoid+garnet+chlorite (Sample 49g). As temperature increases to T_2, the three phase assemblage chloritoid + garnet + staurolite shifts to lower Mn until chloritoid is consumed leaving the garnet+staurolite+chlorite sub-assemblage (Sample 47b).

As it can be seen, the appearance of staurolite is not the result of a garnet consuming reaction such as garnet + chlorite = staurolite + biotite +H_2O, as in low-Al pelites (because biotite is not formed in the studied rocks). Therefore, we conclude that garnet in these samples did not experience any dissolution due to the appearance of staurolite.
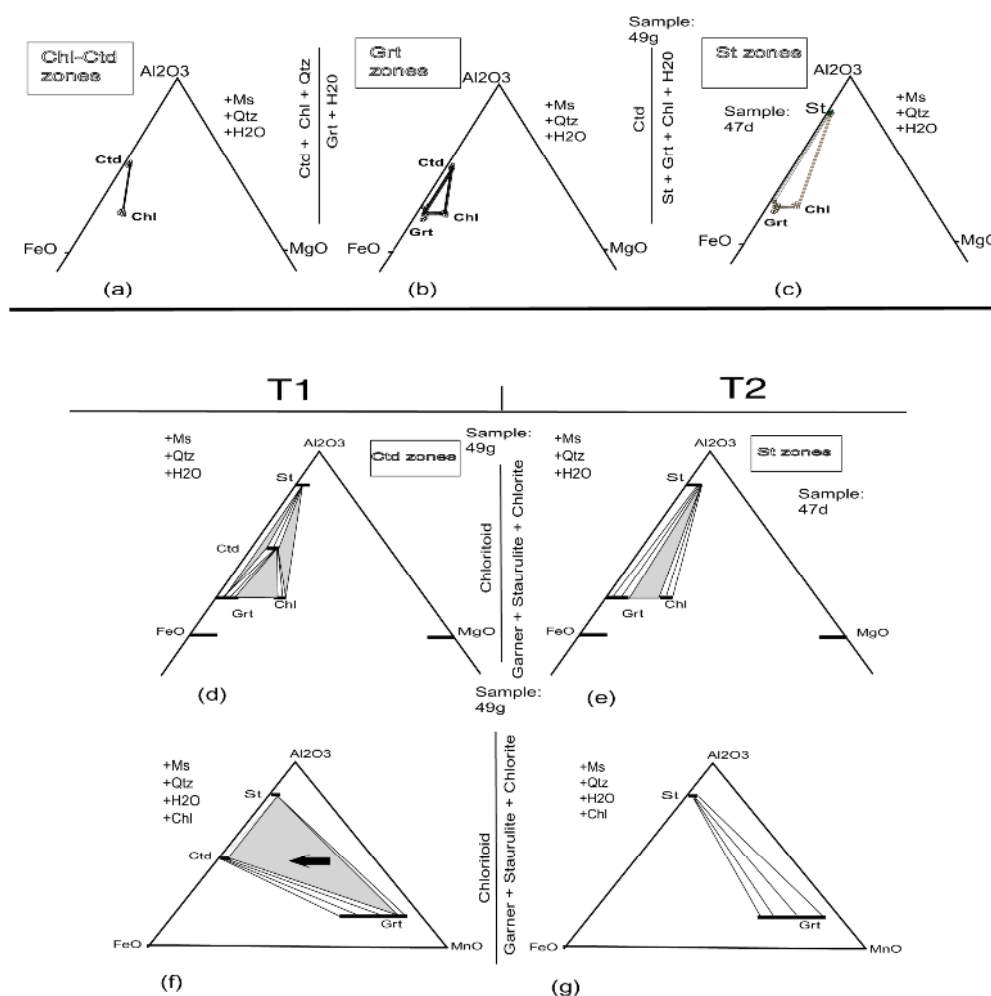

Fig. 8. a,b,c, Al_2O_3-FeO-Mgo projection from quartz, muscovite and H_2O of coexisting minerals in Non-graphitic schists of the Poshtuk sub-area. d,e,f,g, AFMn plots showing the phase relation for the garnet zone and staurolite zone samples.

6- Conclousion

The main mineral assemblage of peak metamorphism in the graphitic metapelites (chloritoid-free schist) of the Bolandparchin is garnet, fibrolite, biotite, muscovite and quartz.

Chloritoid-bearing metapelites of the Poshtuk sub-area contain the assemblage of garnet, staurolite, chlorite, muscovite, chloritoid and quartz;

AFM compatibility diagrams, constructed based on real minerals chemistry, show the phase relations for the garnet zone to sillimanite zone in the chloritoid-free metapelites. The isograds are typical Barrovian type.

AFM and AFMn compatibility diagrams show the phase relations for the garnet zone and staurolite zone samples in the chloritoid-bearing metapelites. The deduced isograds based on the field geology studies and petrographical inspection of the samples are not typical Barrovian type, but reflect the first appearance of chloritoid minerals in these aluminous bulk compositions.

Since biotite is not crystallized in the studied samples, the appearance of staurolite can not be attributed to the garnet consuming reactions as happens in most of the low Al-pelites of the world. Therefore there is two distinct mechanisms for staurolite crystallization in the chloritoid- bearing and chloritoid-free rock studied here.

The stable garnet zone assemblage is chloritoid + garnet + chlorite. As temperature increases the three phase assemblage chloritoid +garnet + staurolite shifts to lower Mn contents until chloritoid is consumed leaving the garnet + staurolite + chlorite assemblage.

Acknowledgements

References
[1] Thompson Jr. J.B., (1957). *"The graphical analyses of mineral assemblages in pelitic schists"*, American Mineralogist, 42, 842-858.

[2] Alavi M., (1991). *"Tectonic map of the Middle East: Geologic Survey of Iran"*, scale 1:5,000,000.

[3] Berberian M., (1981). *"Active faulting and tectonics of Iran"*, in Gupta, H. K., and Delany, F. M., editors, Zagros-Hindu Kush Himalaya Geodynamic Evolution: American Geophysical Union Geodynamic Series, v. 3, p. 33-69.

[4] Ramezani J., Tucker R.D., *"The Saghand region, central Iran: U-Pb geochronology, petrogenesis and implications for Gondwana tectonics"*, [American Journal of Science, Vol. 303, September, 2003, P. 622–665].

[5] Pelissier G., Bolourchi M.H., (1967). *"East Takab metamorphic complex"* (unpublished).

[6] Kretz R., (1983) *"Symbols for rock forming minerals"*, Am. Mineral. 68: 227-279.

[7] Saad N. A, Bouseily K., Kalil (1996) *"Alteration pattern in the Rugs gold mine area, Egypt"*, Acta Mineral. Petrographici XXXVII, 5/-74.

[8] Laird J., (1988). *"Chlorites: metamorphic petrology. In: Hydrous phyllosilicates (ed Bailey, S. W.)"*, Reviews in Mineralogy, 19, 405-453, Mineralogical Society of America.

[9] Lambert R. St. J., (1959). *"The mineralogy and metamorphism of the Moine schists of The Morar and Kroydart districts of Inverness-shire"*, Transactions of the Royal Society of Edinburgh,63, 553.

[10] Mather J. D., (1970). *"The biotite isograde and the lower greenschist facies in the Dalradian rocks of Scotland"*, J. of Petrology, 11, 253-275.

[11] Wang G.-F., Banno S., Takeuchi K., (1986). *"Reactions to define the biotite isograde in the ryoke metamorphic belt, Kii Peninsula"*, Japan. Contributions to Mineralogy and Petrology, 93, 9-17.

[12] Dempester T.J., Tanner P.W.G., (1997). *"The biotite isograd"*, Central Pyrenees: a deformation-controlled reaction. Journal of Metamorphic Geology,15, 531-584.

[13] Robinson P. R., Hollocher K. T., Tracy R.J., Dietsch C.W., (1982). *"High grade Acadian regional metamorphism in south - central Massachusetts. In: NEIGC 74th Annual Meeting of the state Geological and Natural History Survey of Connecticut"*, guidebook for fieldtrips in Connecticut and South-Central Massachusetts (eds Joester, R.A & Quarrier, S.S.), 289-340, The Univercity of Connecticut, Storrs.

[14] Bucher K., Frey M., (1994). *"Petrogenesis of metamorphic Rocks"*, sixth ed.

[15] Spear FS (1993) Metamorphic phase equilibria and pressure-temperature-time paths. Min Soc Am. Mono. Ser. 1, 799 p.

[16] Wang P., Spear F.S., *"A field and theoretical analysis of garnet+chloritoid+chlorite+biotite assemblages from the Tristate (MA, CT, NY) area"*, U.S.A. Cntribution to Mineralogy and Petrology (1991), 106,217-253.

[17] Spear, F. S. & Cheney, J. T., (1989). *"Petrogenetic grid for politic schists in the system SiO2-Al$_2$O$_3$-FeO-MgO-K$_2$O-H$_2$O"*, Contribution to Mineralogy and Petrology, 101, 149-164.

[18] Carmichael D.M., (1970). *"Intersecting isograde in the Wheatstone lake Area Ontario"*, Journal of petrology 11, 147-181.

[19] Yardley B. W. D., 1989. *"An interdiction to metamorphic petrology. Longman Scientific & Technical"*, 248 pp.

[20] Graebner T., Schenk V., (1999) *"Low-pressure metamorphism of Palaeozoic pelites in the Aspromonte"*, Southern Calabria: constraints for the thermal evolution in the Calabrian crustal cross-section during the Hercynian orogeny, J. metamorphic Geol., 1999, 17, 157-172.

[21] Rios C., Garcia C., Takasu A., (2003). *"Tectono-metamorphic evolution of the Silgara Formation metamorphic rocks in the southwestern Santander Massif, Colombian Andes"*, Journal of South American Earth Sciences 16, 133-154.

[22] Thomson J.B., Norton S.A., (1968). *"Paleozoic regional metamorphism in New England and adjacent areas. In Zen, E-An, et al., (Eds): Studies of Appalachian geology"*, Interscience Publisher. John Wiley, New York.

[23] Ganguly J. (1969). *"Chloritoid stability and related parageneses: theory, experiments and applications"*, American Journal of Science 267, 910-944.

[24] Droop G. T. R., Harte B., *"The effect of Mn on the phase relations of Medium-Grade pelites: Constraints from natural assemblages on petrogenetic grid topology"*, (1995).

[25] Saki A., Moazzen M., Moayyed M. (2004). *"Geothermobarometry of metapelites of southwest Mahneshan, Iranian Journal of Crystallography and Mineralogy"*, Vol 12, No 2, 215-230.